AIP | Physics of Plasmas

Predictions of the poloidal asymmetries and transport frequencies in KSTAR

C. Bae, W. M. Stacey, S. G. Lee, and L. Terzolo

Citation: Physics of Plasmas (1994-present) **21**, 012504 (2014); doi: 10.1063/1.4848175
View online: http://dx.doi.org/10.1063/1.4848175
View Table of Contents: http://scitation.aip.org/content/aip/journal/pop/21/1?ver=pdfcov
Published by the AIP Publishing

Predictions of the poloidal asymmetries and transport frequencies in KSTAR

C. Bae,[1,a)] W. M. Stacey,[2] S. G. Lee,[1] and L. Terzolo[1]
[1]National Fusion Research Institute, Gwahak-ro, Yuseong-gu, Daejeon 305-806, South Korea
[2]Fusion Research Center, Georgia Institute of Technology, Atlanta, Georgia 30332, USA

(Received 2 September 2013; accepted 18 November 2013; published online 8 January 2014)

The extended neoclassical rotation theory formulated in Miller flux surface geometry enables unprecedented neoclassical calculations of the poloidal asymmetries in density, rotation velocities, electrostatic potential along the flux surfaces, and of the inertial (Reynolds stress) and gyroviscous transport frequencies, which are strong functions of these asymmetries. This paper presents such calculations of the poloidal asymmetries and non-negligible inertial and gyroviscous transport frequencies in two KSTAR (Korea Superconducting Tokamak Advanced Research) [Kwon *et al.*, Nucl. Fusion **51**, 094006 (2011)] Neutral Beam Injection H-mode discharges. The in-out asymmetries in the velocities are an order of magnitude larger than their up-down asymmetries. The magnitudes of the predicted inertial and gyroviscous transport frequencies depend on the magnitudes of the density and velocity asymmetries. The neoclassically predicted density asymmetries are shown to correspond with the reported measurements in tokamaks and the predicted carbon toroidal velocities agree very well with the measurements in KSTAR. © *2014 AIP Publishing LLC*. [http://dx.doi.org/10.1063/1.4848175]

I. INTRODUCTION

It is important to understand plasma rotation in tokamaks because of the effect of rotation on stabilizing MHD modes[1,2] and confinement.[3,4] To this end, an extended neoclassical rotation theory[5,6] incorporating poloidal asymmetries in density, rotation velocities, and electrostatic potential was recently extended[7,8] to an elongated poloidally asymmetric and Shafranov-shifted flux surface geometry[9,10] and shown to agree rather well with experiment.[7] The extended theory[5 8] is based on the Braginskii's closure theory and viscosity representation[11] and the Stacey-Sigmar (S-S) representation of the poloidal asymmetries and poloidal rotation with low order Fourier series expansions.[12,13]

Existence of the poloidal variations along the flux surfaces in density (and by implication via momentum balance in the velocities and electrostatic potential) has been observed in tokamak experiments[14 17] (primarily in the edge); thus, theoretical understanding of these asymmetries and their contribution to transport and confinement became increasingly important for understanding tokamak plasmas. It was found in Ref. 7 that the accuracy of the extended neoclassical rotation theory[5 8] was sensitive to the accuracy of the flux surface geometry representation. The code written to solve the extended rotation theory,[7,8] GTROTA,[18] has recently been upgraded to allow the calculation of additional plasma parameters not presented in Refs. 5 and 7. The prediction capability of the assumed poloidal asymmetries in density, rotation velocity (both toroidal and poloidal), and electrostatic potential is exploited in this paper to calculate all these asymmetries in two KSTAR (Korea Superconducting Tokamak Advanced Research)[19] H-mode discharges and to estimate from them the inertial (Reynolds stress) and gyroviscous transport frequencies that would affect rotation. Evaluating the transport frequencies as functions of the asymmetries based on an elongated flux surface geometry representation, the predicted carbon toroidal rotation velocities presented in this paper for the two KSTAR shots agree very well with the measurements, as they did previously for two DIII-D discharges.[7] This paper presents the calculated results of the asymmetries and the transport frequencies, which contributed to the accuracy in the velocity predictions and discusses the importance of the poloidal asymmetries and their impact on the main ion and impurity transport in tokamaks.

II. EXTENDED NEOCLASSICAL ROTATION THEORY

A. Plasma fluid equations

Based on the Braginskii's closure theory,[11] the extended rotation theory[5 8] is developed from the continuity and momentum balance equations for a two-ion species plus electron plasma model, yielding a set of coupled equations to solve for the radial profiles of the mean velocities and the up-down and in-out asymmetries in density, toroidal and poloidal velocities, and the electrostatic potential. The viscosity model is based on the Braginskii's flow rate of strain[11] extended to toroidal geometry by Stacey and Sigmar,[20] to the Miller flux surface model by Stacey and Bae,[21] and extended to arbitrary collisionality by the use of the Shaing-Sigmar neoclassical viscosity model.[13] Eq. (1) shows the basic form of the momentum balance equation in the extended rotation theory[5 8] in a coordinate-free form

$$n_j m_j \left(\vec{V}_j \cdot \nabla\right)\vec{V}_j + \nabla P_j + \nabla \cdot \vec{\pi}_j \\ n_j e_j (\vec{E} + \vec{V}_j \times \vec{B}) + \vec{F}_j^{\,1} + \vec{S}_j^{\,1} \quad m_j \vec{V}_j S_j^{\,o}. \qquad (1)$$

The first term in Eq. (1) comes from the Reynolds stress, $n_j m_j \nabla \cdot \left(\vec{V}_j \vec{V}_j\right)$, and is called "inertial" term in the extended rotation theory.[5 8] Note that this inertial term is usually neglected in neoclassical studies but the extended rotation theory[5 8] not only retains it but also evaluates its contribution

a)Electronic mail: cbae@nfri.re.kr

as a function of the up-down velocity asymmetry as presented in this paper. The extended rotation theory[5 8] decomposes Eq. (1) into three scalar components (r, θ, ϕ) and converts them into the curvilinear geometry with the method discussed by Stacey and Bae.[21] More details on the recent derivation of the extended rotation theory[7,8] with a realistic flux surface geometry[10] can be found in Refs. 7 and 8.

The very characteristics of the extended rotation theory[5 8] that allow predictions of the poloidal asymmetries and the related transport come from the uniqueness of the S-S poloidal rotation model,[12,13] which takes additional physics factors into account compared to the Hirshman-Sigmar (H-S) model[22] that NCLASS code[23] is based on. These characteristics include: (1) inclusion of all the terms in the poloidal momentum balance equation including the nonlinear "inertial" term; (2) the lowest order Fourier series expansion of density, velocity, and electrostatic potential; and (3) calculation of the inertial and gyroviscous transport as functions of the poloidal asymmetries. Inclusion of all the terms in the poloidal component of the momentum balance, Eq. (1), is especially important for an accurate calculation of the poloidal velocity and the asymmetries along the flux surfaces. The final form of the poloidal momentum balance equation in the S-S model[12,13] is shown in Eq. (2) in curvilinear geometry with the sources (S_j^{ρ} and $\vec{S}_j^{1}$) and friction ($\vec{F}_j^{1}$) replaced with the actual calculation models

$$\begin{aligned} & n_j m_j \left[\left(\vec{V}_j \cdot \nabla \right) \vec{V}_j \right]_\theta + \left(\nabla \cdot \vec{\pi}_j \right)_\theta + \frac{1}{h_\theta} \frac{\partial p_j}{\partial \theta} \quad M_{\theta j} \\ & \quad + n_j m_j \nu_{jk} (V_{\theta j} \quad V_{\theta k}) + n_j e_j (V_{rj} B_\phi \quad E_\theta) \\ & \quad + n_j m_j \nu_{ionj} V_{\theta j} + n_j m_j \nu_{elcxj} V_{\theta j} \quad 0, \end{aligned} \tag{2}$$

where h_θ is the differential metric coefficient in the poloidal coordinate. Here, M_j is the external momentum input and the fifth term is the interspecies collisional friction given by a Lorentz form, $\vec{F}_j^{1} \quad n_j m_j \sum_k \nu_{jk} (\vec{V}_j \quad \vec{V}_k)$. The lowest order Fourier expansion of density, velocity, and electrostatic potential in the S-S model[12,13] is of the form

$$X_j(r,\theta) \approx \bar{X}_j(r) \left[1 + X_j^c(r) \cos\theta + X_j^s(r) \sin\theta \right], \tag{3}$$

for a given plasma parameter X of the species j with the overbar indicating the average over the flux surface at a given radial location (r). The superscript "c" and "s" indicate poloidally "in-out" and "up-down" variations of the parameter X along the flux surface. Thus, the coefficients $(n_j^{c,s}, V_{\theta_j,\phi_j}^{c,s}, \Phi^{c,s})$ introduced from the sine and cosine expansions in Eq. (3) are termed "poloidal asymmetries" in the extended rotation theory[5 8] and can be calculated as functions of the radial coordinate. The final formalism couples the velocity $(V_{\theta_j,\phi_j}^{c,s})$ and electrostatic potential asymmetries $(\Phi^{c,s})$ to the density asymmetries $(n_j^{c,s})$; thus, the expansions given in Eq. (3) introduce $n_j^{c,s}$ only as the new unknown variables in the final numerical calculation model,[18] which constitutes an eight coupled nonlinear set of equations for a two-ion plus electron plasma model. The third characteristic of the S-S model,[12,13] calculation of the inertial and gyroviscous transport frequencies as functions of the asymmetries, is simply a direct consequence of the expansions assumed in Eq. (3) as presented in the Sec. II B.

B. Transport frequencies and poloidal asymmetries

The extended rotation theory[7,8] with a realistic flux surface geometry[10] and the Shafranov shifts[9] presents the formalism that allows predictions of the cross-field toroidal angular momentum transport processes, which are represented by the inertial and gyroviscous transport frequencies (ν_{nj} and ν_{dj}, respectively). From the toroidal angular momentum component of the first term in Eq. (1), the flux surface average (FSA) of toroidal angular "inertial" torque with the Miller geometry[10] is given by

$$\langle n_j m_j R^2 \nabla\phi \cdot \left(\vec{V}_j \cdot \nabla \right) \vec{V}_j \rangle \quad R_0 \bar{n}_j m_j \nu_{nj} \bar{V}_{\phi j}, \tag{4}$$

with the inertial (Reynolds stress) transport frequency given by

$$\begin{aligned} \nu_{nj} \approx & \frac{\bar{V}_{rj}}{R_0} \left[\frac{\partial R_0}{\partial r} \left\langle \frac{1}{h_r} \right\rangle + \left\langle \frac{\cos\xi}{h_r} \right\rangle \quad R_0 L_{V_\phi}^{-1} \right] \\ & + \bar{V}_{\theta j} \varepsilon \bar{V}_{\phi j}^{s} \left(\left\langle \cos\theta \frac{1}{h_\theta} \right\rangle + \frac{\left\langle \frac{1}{R} \frac{\partial R}{\partial \theta} \sin\theta \frac{1}{h_\theta} \right\rangle}{\left\langle \sin^2\theta \frac{1}{h_\theta} \right\rangle} \left\langle \cos^2\theta \frac{1}{h_\theta} \right\rangle \right. \\ & \left. + \varepsilon \left\langle \cos\theta \frac{\cos\xi}{h_\theta} \right\rangle + \frac{1}{R_0} \left\langle \frac{\partial R}{\partial \theta} \sin\theta \frac{1}{h_\theta} \right\rangle \right), \end{aligned} \tag{5}$$

where $\partial R_0/\partial r$ represents the Shafranov shift,[9] L_X^{-1} $1/X(\partial X/\partial r)$ is the gradient length scales for a given quantity X, h_r is the differential metric coefficient in the radial coordinate, $\varepsilon \_ r/R_0$, and $\bar{V}_{\phi j}^{c,s} \_ V_{\phi j}^{c,s}/\varepsilon$ is the normalized toroidal velocity asymmetries used in the numerical calculation model.[18] Note that the first term in Eq. (5) is independent of the poloidal asymmetries but the second one is a strict function of $V_{\phi j}^{s}$; thus, any neoclassical theory without $\bar{V}_{\phi j}^{c,s}$ in its formalism will not calculate this contribution unless formulated otherwise. Also from the toroidal angular momentum of the second term in Eq. (1), the FSA of toroidal angular "viscous" torque is given by

$$\begin{aligned} \langle R^2 \nabla\phi \cdot \nabla \cdot \vec{\pi} \rangle \quad & \langle \left(R^2 \nabla\phi \cdot \nabla \cdot \vec{\pi} \right)_\perp \rangle + \langle \left(R^2 \nabla\phi \cdot \nabla \cdot \vec{\pi} \right)_{gv} \rangle \\ & \approx \langle \left(R^2 \nabla\phi \cdot \nabla \cdot \vec{\pi} \right)_{gv} \rangle \quad R_0 \bar{n}_j m_j \nu_{dj} \bar{V}_{\phi j}, \end{aligned} \tag{6}$$

where the gyroviscous (drag) transport frequency is given by

$$\nu_{dj} \approx \nu_{dj}^{1} + \nu_{dj}^{2}, \tag{7}$$

with the first term representing the contribution of the elongated geometry[10] alone and the second term from the gradient scales being the similar result obtained in the earlier circular flux surface model[5,6]

$$\nu^1_{\bar{d}j} \quad \frac{T_j}{R_0^2 e_j \bar{B}_\phi}\varepsilon\left[\begin{array}{l}\bar{V}^s_{\phi j}\left(2R_0\left\langle\cos\theta\frac{\cos\xi}{h_\theta h_r}\right\rangle+\left\langle R\cos\theta\frac{\cos\xi}{h_\theta h_r}\right\rangle+\left\langle R\sin\theta\frac{\sin\xi}{h_\theta h_r}\right\rangle+x\left\langle R\sin\theta\cos\theta\frac{\sin\xi}{h_\theta h_r}\right\rangle\right)\\ +\bar{n}^s_j\left(\left\langle R\sin\theta\frac{\sin\xi}{h_\theta h_r}\right\rangle+x\left\langle R\sin\theta\cos\theta\frac{\sin\xi}{h_\theta h_r}\right\rangle\right)\end{array}\right], \tag{8}$$

$$\nu^2_{\bar{d}j} - \frac{1}{2}\frac{\bar{\theta}_j G_j T_j}{R_0{}^2 e_j \bar{B}_\phi}, \tag{9}$$

where

$$G_j - r\left(L^{-1}_{n_j}+L^{-1}_{T_j}+L^{-1}_{V_{\phi j}}\right), \tag{10}$$

$$\bar{\theta}_j \quad 2\varepsilon\left[\begin{array}{l}\bar{V}^s_{\phi j}\left(\bar{n}^c_j\left\langle R\frac{\cos^2\theta}{h_\theta h_r}\right\rangle+\frac{1}{\varepsilon}\left\langle R\frac{\cos\theta}{h_\theta h_r}\right\rangle+\left\langle R\cos\theta\frac{\cos\xi}{h_\theta h_r}\right\rangle+\left\langle R\sin\theta\frac{\sin\xi}{h_\theta h_r}\right\rangle+x\left\langle R\sin\theta\cos\theta\frac{\sin\xi}{h_\theta h_r}\right\rangle\right)\\ +\bar{n}^s_j\left(\quad \bar{V}^c_{\phi j}\left\langle R\frac{\sin^2\theta}{h_\theta h_r}\right\rangle+\left\langle R\sin\theta\frac{\sin\xi}{h_\theta h_r}\right\rangle+x\left\langle R\sin\theta\cos\theta\frac{\sin\xi}{h_\theta h_r}\right\rangle\right)\end{array}\right], \tag{11}$$

with $\bar{n}^{c,s}_j - n^{c,s}_j/\varepsilon$ being the normalized density asymmetries in the numerical calculation model.[18] Equation (6) shows an important characteristic of the extended rotation theory[5 8] that the perpendicular viscosity, which is traditionally believed to dominate most of the neoclassical viscous transport, is simply neglected due to Braginskii's $\eta_{gv} \gg \eta_\perp$ ordering and the gyroviscosity replaces its role of predicting the entire neoclassical viscous damping. Note here that $\nu_{\bar{d}j}$ given by Eqs. (7)–(11) is a strong function of $n^{c,s}_j$ and $V^{c,s}_{\phi j}$, thus vanishes in any formalism that neglects the corresponding poloidal variations unless formulated otherwise. In the extended neoclassical rotation theory,[7,8] $V^{c,s}_{\theta j}$ and $\Phi^{c,s}$ do not play a direct role in the calculation of ν_{nj} and $\nu_{\bar{d}j}$ but affect the final results through their couplings with other plasma parameters.

The extended rotation theory[7,8] takes the cosine and sine moments of Eq. (2) with the Fourier expansions assumed in Eq. (3), which reduce to Eqs. (12) and (13), respectively (expressed in generic forms for the two species, with j being either i *deuterium* or I *carbon* and k being the other), to solve for $\bar{n}^{c,s}_j(r)$

$$A_{C1}\bar{n}^c_j + A_{C2}\bar{n}^s_j + A_{C3}\bar{n}^c_k \quad B_C, \tag{12}$$

$$A_{S1}\bar{n}^c_j + A_{S2}\bar{n}^s_j + A_{S3}\bar{n}^s_k \quad B_S, \tag{13}$$

where $A_{C,S}$ and $B_{C,S}$ coefficients can be found in Appendix C of Ref. 7. All other asymmetries, $V^{c,s}_j$ and $\Phi^{c,s}$, are coupled to $n^{c,s}_j$ by

$$\bar{V}^s_{\theta j} - V^s_{\theta j}/\varepsilon \quad \bar{n}^s_j, \tag{14}$$

$$\bar{V}^c_{\theta j} - \frac{V^c_{\theta j}}{\varepsilon} \quad \bar{n}^c_j + \frac{1}{\varepsilon}\left\langle\frac{1}{R}\frac{\partial R}{\partial\theta}\sin\theta\frac{1}{h_\theta}\right\rangle\Big/\left\langle\sin^2\theta\frac{1}{h_\theta}\right\rangle, \tag{15}$$

$$\bar{V}^s_{\phi j} \quad \bar{n}^s_j\alpha^{1S}_j + \alpha^{2S}_j, \tag{16}$$

$$\bar{V}^c_{\phi j} \quad \frac{\hat{V}_{\theta j}}{\hat{V}_{\phi j}}\left(\alpha^{3C}_j + \alpha^{2C}_j\frac{\left\langle\frac{1}{1+\varepsilon\cos\xi}\right\rangle}{\left\langle\frac{1}{h_r}\right\rangle}\right) + \alpha^{1C}_j \quad \alpha^{2C}_j \times\left(1+\frac{\partial R_0(r)}{\partial r}\right)\frac{\left\langle\frac{1}{(1+\varepsilon\cos\xi)}\frac{1}{h_r}\right\rangle}{\left\langle\frac{1}{h_r}\right\rangle} \quad \frac{\hat{P}'_j}{\hat{V}_{\phi j}}\left(\alpha^{2C}_j \quad \alpha^{4C}_j\right), \tag{17}$$

$$\bar{\Phi}^{c,s} - \frac{\Phi^{c,s}}{\varepsilon} \quad \frac{T_e\bar{n}^{c,s}_e}{\bar{\Phi}e}, \tag{18}$$

where α^{1S}_j, α^{2S}_j, α^{1C}_j, α^{2C}_j, α^{3C}_j, and α^{4C}_j can be found in Appendix C of Ref. 7 and $\bar{n}^{c,s}_e - n^{c,s}_e/\varepsilon$ are coupled with $\bar{n}^{c,s}_j$ by the charge neutrality, $\bar{n}_e \approx Z_j\bar{n}_j + \sum_k Z_k\bar{n}_k$. Note that all the parameters in Eqs. (14) to (18) are normalized to the same order of magnitude in the numerical computation model.[18] Therefore, the formalism presented in this section allows calculations of the poloidal asymmetries assumed in the S-S model,[12,13] and the associated inertial and gyroviscous transport frequencies that represent the cross-field momentum transfer for two KSTAR H-mode discharges introduced in the Sec. III.

III. KSTAR EXPERIMENTS

Two similar KSTAR NBI (Neutral Beam Injection) H-mode discharges (#5505 and #5953) are analyzed in this paper to calculate the poloidal asymmetries and transport frequencies in order to investigate their relative magnitudes. Table I summarizes the discharge parameters and the experimental configuration for both shots is illustrated in Fig. 1, which is a typical KSTAR experimental setup with the plasma current in CW (clockwise) direction. KSTAR currently has no poloidal velocity (V_θ) measurement capability and toroidal rotation is measured by both XICS (X-Ray

TABLE I. Summary of the KSTAR shot parameters.

Shot properties	Shot 5505 (2500 ms)	Shot 5953 (2500 ms)
Beam injection direction	Co-injection	Co-injection
Divertor configuration	Lower single null (USN)	Lower single null (LSN)
R (major radius)	1.832 m	1.835 m
a (minor radius)	0.504 m	0.488 m
$B_\phi(r=0)$ (toroidal B field)	1.91 T	1.91 T
B_θ^{max} (max. poloidal B field)	0.16 T	0.21 T
$\kappa(r=a)$ (elongation)	1.821	1.85
$\delta(z_{bottom})/\delta(z_{top})$ (triangularity)	0.8/0.511	0.761/0.486
I (current)	0.661 MA	0.613 MA
V_{loop} (loop voltage)	0.233 V	0.248 V
NBI power	90 keV	85 keV
Impurity/deuterium density ratio	0.11	0.11

Imaging Crystal Spectrometer) and CES (Charge Exchange Spectroscopy). For the two shots analyzed in this paper, however, CES measurements were not available due to no beam modulations. Thus, toroidal velocity (V_ϕ) measurements were available for the core range only ($\rho < 0.2$ for #5505 and $\rho < 0.4$ for #5953, where $\rho \quad r/a$ is the normalized radial distance) through XICS but with a highly reliable accuracy. KSTAR injects puffed argon gas for XICS to measure V_ϕ^{Ar}; thus, we initially assume $V_\phi^{Ar} \approx V_\phi^{Carbon}$ and iterate the nonlinear algorithm in GTROTA[18] to predict both toroidal and poloidal velocities of both carbon impurity and deuterium. GTROTA[18] was also modified to test the validity of the calculated V_θ profiles by checking the final solutions with different initial guesses inferred from TRANSP data.

IV. PREDICTIONS OF VELOCITIES AND ASYMMETRIES

A. Predicted velocities

Fig. 2 shows the toroidal (Vt) and poloidal (Vp) velocities predicted by GTROTA[18] for the two KSTAR discharges. The predicted toroidal carbon velocities (Vt_C^{comp}) are

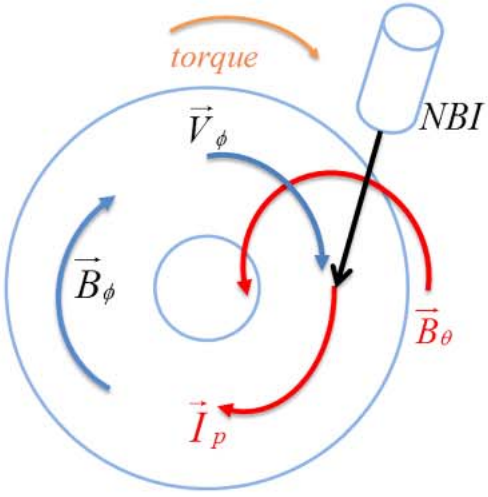

FIG. 1. KSTAR experimental setup (shots #5505 and #5953).

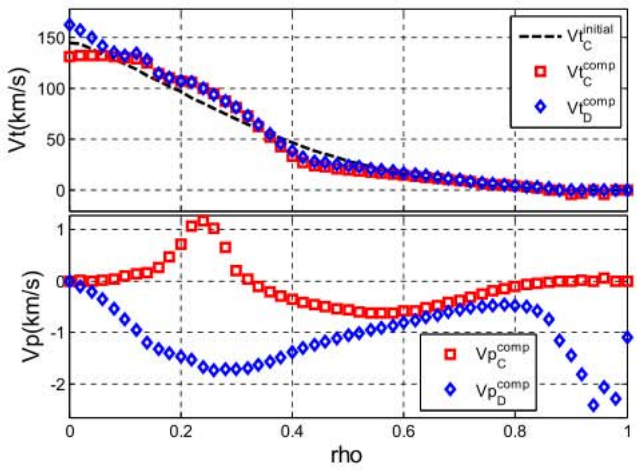

a) #5505(2500ms)

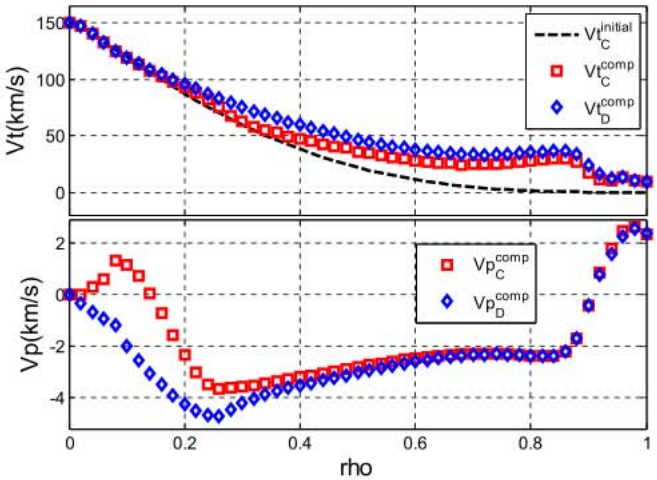

b) #5953(2500ms)

FIG. 2. Toroidal and poloidal velocities in two KSTAR discharges (positive CW when viewed from the top for Vt/positive upward at outboard midplane for Vp). (a) #5505 (2500 ms); (b) #5953 (2500 ms).

shown to stay within approximately <10% to the experimentally measured profiles ($Vt_C^{initial}$) in the core ranges ($\rho < 0.2$ for #5505 and $\rho < 0.4$ for #5953), which is the same finding as in Ref. 7. The $Vt_C^{initial}$ profiles in the range with no measurements are simply interpolated against the measured temperature so that we have the initial guesses for the nonlinear GTROTA algorithm[18] for the entire radial range. Thus, the seemingly large deviation in the $\rho > 0.4$ range for #5953 does not indicate that the final solution actually deviates from the measurement. It rather indicates that the predicted Vt_C^{comp} profile is a more reliable than the interpolated one in the non-measured range. We also note that the velocity profiles shown in Fig. 2 are not reliable in the edge ($\rho > 0.9$) with the current theory[7,8] due to lack of sophisticated atomic physics treatment in the edge.

A test of the numerical calculation with the asymmetries turned off shows over-predictions of Vt_C^{comp} when compared to $Vt_C^{initial}$ in the measured core ranges, proving the importance of the asymmetries in the S-S model[20] and the inertial and gyroviscous damping contributions calculated to counter the over-predictions. This test indirectly compares the S-S

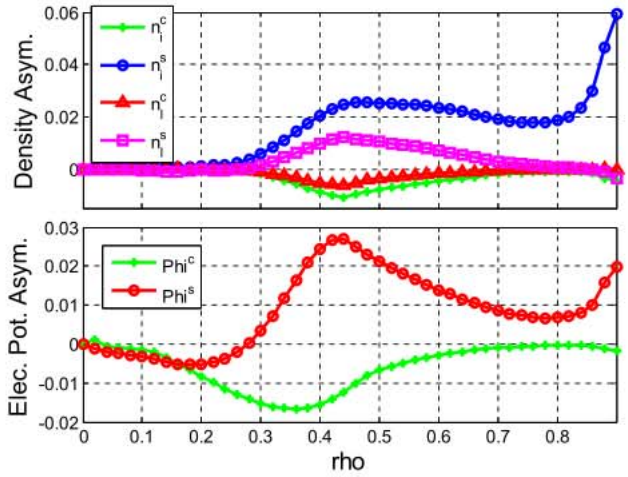

a) Density and electrostatic potential asymmetries

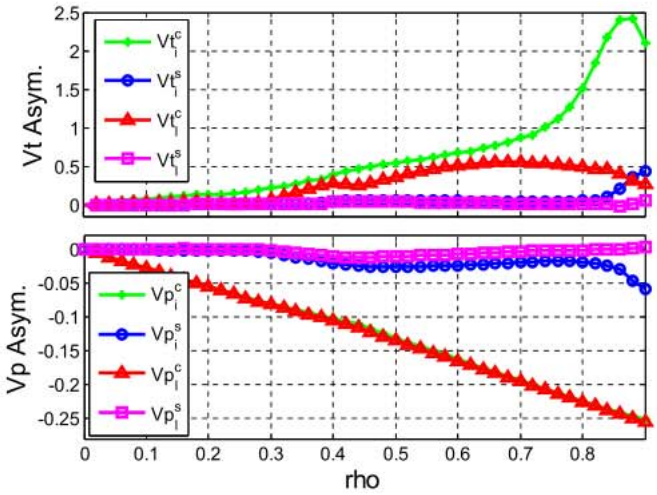

b) Toroidal and poloidal velocity asymmetries

($i = deuterium / I = carbon$)

FIG. 3. Poloidal asymmetries of KSTAR #5505 (2500 ms) discharge. (a) density and electrostatic potential asymmetries; (b) toroidal and poloidal velocity asymmetries ($i = deuterium/I = carbon$).

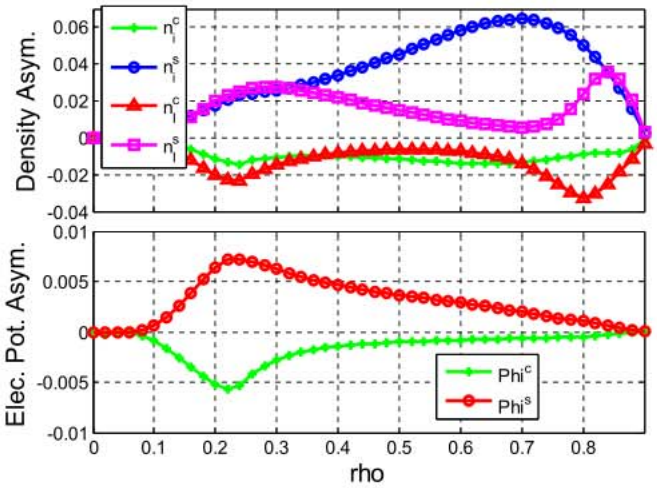

a) Density and electrostatic potential asymmetries

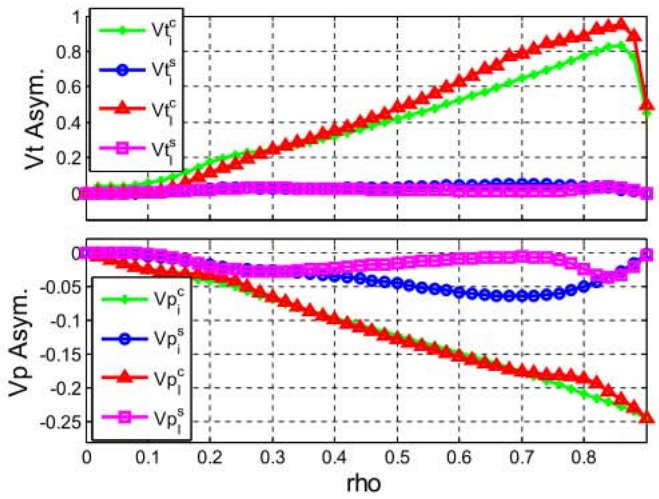

b) Toroidal and poloidal velocity asymmetries

($i = deuterium / I = carbon$)

FIG. 4. Poloidal asymmetries of KSTAR #5953 (2500 ms) discharge. (a) Density and electrostatic potential asymmetries. (b) Toroidal and poloidal velocity asymmetries ($i = deuterium/I = carbon$).

model and the H-S model, i.e., GTROTA and NCLASS, respectively, but even with the asymmetries turned off the extended rotation theory[5,8] contains more terms, including the nonlinear "inertial" term, than NCLASS does. In addition, the realistic flux surface geometry using the Miller model and Shafranov shifts are accounted for in GTROTA. A direct comparison between NCLASS and GTROTA calculations is expected to be available in the near future. GTROTA is also expected to be upgraded to allow predictions of the velocities based on diverse theoretical settings such as circular or Miller geometry with and without poloidal asymmetries, which would allow investigation of both geometry and poloidal asymmetry effects in neoclassical calculations.

B. Predicted poloidal asymmetries

Figs. 3 and 4 show all the calculated poloidal asymmetries for the reliable range ($\rho < 0.9$) with the current theory.[7,8] It is shown that the density asymmetries ($n_j^{c,s}$) are generally of $\sim O(10^{-2})$ for the $\rho < 0.9$ range but usually of larger magnitudes in the edge ($\rho > 0.9$) although the edge data are not presented in Figs. 3 and 4 to prevent misleading. Though n_j^c and n_j^s stay within the same order of magnitude, n_j^s is generally larger than n_j^c for the two discharges. Recent experiments in the C-Mod[14,15] suggest $O(10^0)$ in the edge for $n_{A_Y}^{c,s}$ from the ohmic discharges but a direct comparison to the GTROTA[18] prediction is not available since the C-mod measurements are mainly for the edge. For an indirect comparison, Reinke *et al.*[14] recently suggested that $n_{A_Y}^s$ in the C-Mod scales with $n_e B_\phi / I_p$ factor and the impurity distribution transitions from a nearly symmetric state (<0.1) to a strongly asymmetric state (~1) as $n_e B_\phi / I_p$ increases through $3.5 < n_e B_\phi / I_p < 4$ range. Although the KSTAR discharges analyzed here are not ohmic, their $n_e B_\phi / I_p(MA) \times 10^{-20}$ values are calculated to be approximately 2.2 in the core and monotonically decrease to 0.2 in the edge, thus generally much lower values than the transition threshold of the ohmic discharges in Ref. 14. Thus, the magnitudes of n_I^s predicted by the extended rotation theory[7,8] for the two KSTAR strong

rotation discharges, which are shown to be <0.04 from Figs. 3 and 4, seem to be consistent with the asymmetries observed in the C-Mod.[14]

Existence of the up-down asymmetry in toroidal velocity (V_ϕ^s) is observed in the two KSTAR discharges with their V_ϕ measurements showing different magnitudes in the up and down directions from the plasma center and the calculations presented in Figs. 3 and 4 show that they are in the same order of magnitude with $n^{c,s}$. It is, however, interesting that the in-out asymmetries in both velocities ($V_{\theta,\phi}^c$) are generally larger than the up-down asymmetries ($V_{\theta,\phi}^s$) by an order of magnitude, which is an opposite finding from the case of n_j^c and n_j^s comparison. From Eq. (15), it can be observed that the larger magnitude for V_θ^c is a result of the geometry effect because the second term in Eq. (15) comes from the FSAs of the Miller geometry metric coefficients while the first term (n_j^c) is shown to be an order of magnitude smaller from Figs. 3(a) and 4(a). An investigation of Eq. (17), however, reveals that V_ϕ^c is calculated from a combination of several physical parameters along with the asymmetries, thus not from the geometry effect alone. Another interesting result is that V_ϕ^c of deuterium, Vf_i^c from Fig. 3(b), reaching much larger than 1.0 above $\rho > 0.75$ for #5505 indicates the possible existence of negative toroidal velocities (i.e., flow reversal) at some poloidal locations along its coordinate direction (θ) but its verification is difficult with current diagnostic data. We also note that this large V_ϕ^c asymmetry value must be understood as a tendency, not to predict the magnitude of an effect, because the current theory[7,8] retains only the first order terms in the asymmetries and thus we implicitly neglect the higher order asymmetries and the higher order products of the low order asymmetry terms. With the expected complication of considering the neglected higher order terms and possible other effects such as lack of accuracy in the provided plasma inputs and the numerical noises in the V_ϕ^c calculation using Eq. (17), the V_ϕ^c values being much larger than 1.0 for #5505 indicates a strong tendency for V_ϕ^c to grow in the corresponding range but the actual magnitude must be determined with the higher order terms considered in future calculations.

The electrostatic potential asymmetries ($\Phi^{c,s}$) are generally smaller than $n_j^{c,s}$ by more than an order of magnitude but these smaller $\Phi^{c,s}$ are believed to be as important as other asymmetries in the accuracy of the velocity calculations because the electrostatic potential ($\bar{\Phi}$) has a significant impact in the momentum balance. From the numerical calculations for the two KSTAR strong rotation discharges analyzed, we can conclude

$$\left\{\Phi^{c/s} \le O(10^{-2})\right\} < \left\{n^{c/s} \sim V_{\phi,\theta}^s \sim O(10^{-2})\right\} < \left\{V_{\phi,\theta}^c \sim O(10^{-1})\right\}, \tag{19}$$

and we can fairly expect similar results for the strong rotation discharges in other tokamaks. The small poloidal asymmetries in density and electrostatic potential with their magnitudes at or below $O(10^{-2})$ would simply indicate small physical variations along the poloidal direction in the two KSTAR discharges. The velocity asymmetries, however, indicate significantly complicated physical variations along the flux surfaces with $V_{\theta,\phi}^c$ being much larger in magnitude than $V_{\theta,\phi}^s$. The current KSTAR data indicates the possibility of experimentally measuring $V_{\theta,\phi}^s$ without modifying the diagnostic configuration but the $V_{\theta,\phi}^c$ measurements would require some modification to gain access from both the low-field and high-field sides as done in Ref. 15.

C. Predicted transport frequencies

Fig. 5 presents the calculated inertial (ν_{nj}) and gyroviscous (ν_{dj}) transport frequencies, and their additions ($\nu_{nj} + \nu_{dj}$). A numerical investigation on ν_{nj} shows that the first term in Eq. (5) is smaller than the second by more than an order of magnitude with V_θ being much larger than V_r. Thus, we can approximate Eq. (5) as Eq. (20), indicating that ν_{nj} is a strong function of $V_{\phi j}^s$, thus not negligible even with $V_{\phi j}^s$ being $\sim O(10^{-2})$ as presented in the Sec. IV B and an approximation of $n_j^{c,s}$ alone in the formalism cannot predict this larger contribution to inertial (Reynolds stress) transfer

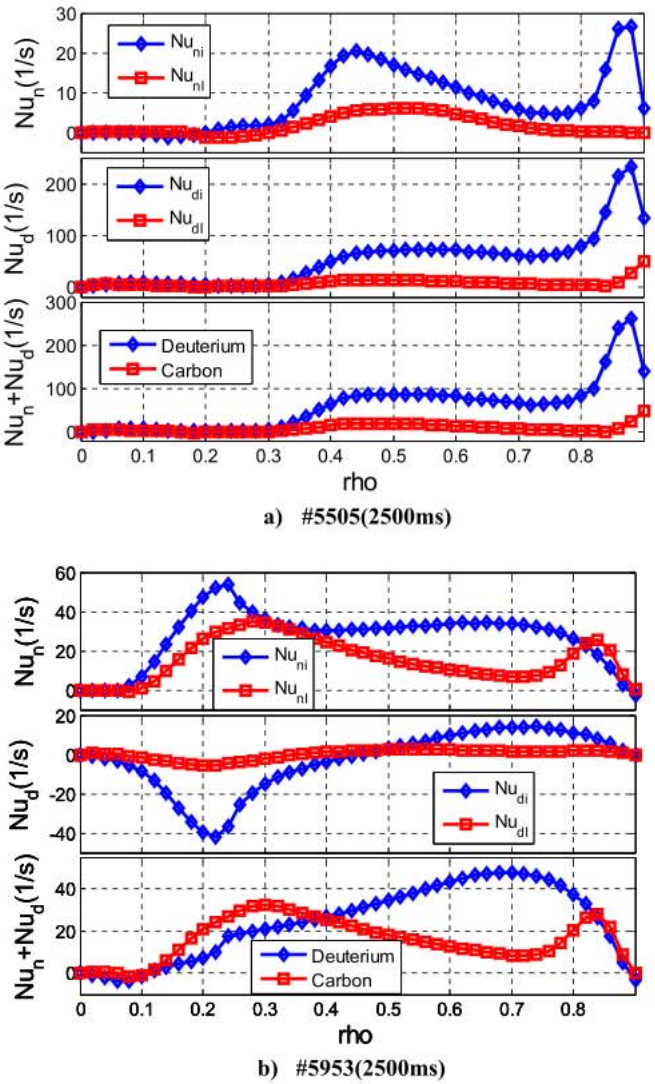

FIG. 5. Transport frequencies of two KSTAR discharges (top: ν_{nj}, middle: ν_{dj}, bottom: the addition of ν_{nj} and ν_{dj}). (a) #5505 (2500 ms); (b) #5953 (2500 ms).

$$\nu_{nj} \approx \bar{V}_{\theta j}\varepsilon\bar{V}^{s}_{\phi j}\left(\left\langle \cos\theta\frac{1}{h_\theta}\right\rangle + \frac{\left\langle \frac{1}{R}\frac{\partial R}{\partial\theta}\sin\theta\frac{1}{h_\theta}\right\rangle}{\left\langle \sin^2\theta\frac{1}{h_\theta}\right\rangle}\left\langle \cos^2\theta\frac{1}{h_\theta}\right\rangle + \varepsilon\left\langle \cos\theta\frac{\cos\xi}{h_\theta}\right\rangle + \frac{1}{R_0}\left\langle \frac{\partial R}{\partial\theta}\sin\theta\frac{1}{h_\theta}\right\rangle\right). \quad (20)$$

For ν_{dj} which is a function of several different asymmetries and other plasma parameters as shown in Eqs. (7) to (11), we note that without the poloidal asymmetries we end up calculating the much smaller perpendicular viscous transport, $\langle(R^2\nabla\phi\cdot\nabla\cdot\vec{\pi})_\perp\rangle$, leading us to believe that the viscous transport is negligible in tokamaks. In the extended rotation theory,[5 8] we neglect this smaller perpendicular viscosity contribution and instead calculate the gyroviscous component, $\langle(R^2\nabla\phi\cdot\nabla\cdot\vec{\pi})_{gv}\rangle$, due to the Braginskii's coefficients ordering given by $\eta_{gv} \gg \eta_\perp$.[11] Compared to ν_{nj}, we observe that $O(\nu_d) \gg O(\nu_n)$ by an order of magnitude for #5505 but $O(\nu_d) \sim O(\nu_n)$ for #5953. A numerical comparison of ν_d^1 and ν_d^2, given by Eqs. (8) and (9) respectively, reveals that these two components show oppositely directed transport; thus, their relative magnitudes determine the final order of magnitude for ν_d. Based on the two KSTAR shots analyzed in this paper, the gyroviscous momentum transport is larger than the Reynolds stress momentum transfer ($\nu_d \gg \nu_n$) when $|\nu_d^2| \gg |\nu_d^1|$ but both are comparable ($\nu_d \sim \nu_n$) when $|\nu_d^2| \sim |\nu_d^1|$. From Eqs. (8) and (9), we see that ν_d^1 is physically coupled with two up-down asymmetries ($V^s_{\phi j}$, n^s_j) while ν_d^2 is associated with the gradient factor (G_j) in Eq. (10) and the asymmetry factor ($\bar{\theta}_j$) in Eq. (11); thus, a combination of both up-down ($V^s_{\phi j}$, n^s_j) and in-out asymmetries ($\bar{n}^c_j$, $\bar{V}^c_{\phi j}$). A numerical investigation on G_j and $\bar{\theta}_j$ reveals that ν_d^2 is dominated by G_j with its magnitude higher than that of $\bar{\theta}_j$ by more than an order of magnitude; thus, physically large gradients in density, temperature, and toroidal velocity profiles seem to yield higher ν_d^2, causing larger gyroviscous transport than the inertial transport ($\nu_d \gg \nu_n$). On the other hand, a unique combination of $V^s_{\phi j}$ and n^s_j may yield relatively high ν_d^1 values, which would reduce the gyroviscous transport to make it comparable to the inertial transport ($\nu_d \sim \nu_n$). This will be further investigated as more shots are analyzed from diverse tokamaks in the future. Fig. 5 also presents the additions of ν_{nj} and ν_{dj}, which show no sign of any "cancellation" between the two. This result suggests that the more detailed approach taken by the S-S rotation model[20] with all the terms retained in the poloidal momentum balance and the representation of the poloidal asymmetries with an accurate geometry effect[10] show no sign of gyroviscous cancellation.

V. RADIAL ELECTRIC FIELDS

Unlike the tokamaks with well-established diagnostics such as DIII-D, KSTAR currently do not have $\bar{V}_\theta$ measurement capability, preventing the calculation of experimental radial electric field ($\bar{E}_r$) profile. This limitation prevents further theoretical researches on numerous interesting KSTAR discharges even though the performance of superconducting KSTAR tokamak is of great interest to the fusion plasma community. GTROTA,[18] however, predicts $\bar{V}_\theta$ profiles (and $\bar{V}_\phi$ in the non-measured range by XICS) of both deuterium and carbon as presented in this paper using its nonlinear iteration scheme, thus allowing a theoretical prediction of $\bar{E}_r$ even with limited velocity measurements. The predicted $\bar{E}_r$ for the two KSTAR discharges presented in Fig. 6 are calculated based on Eq. (21) from the extended rotation theory[7,8]

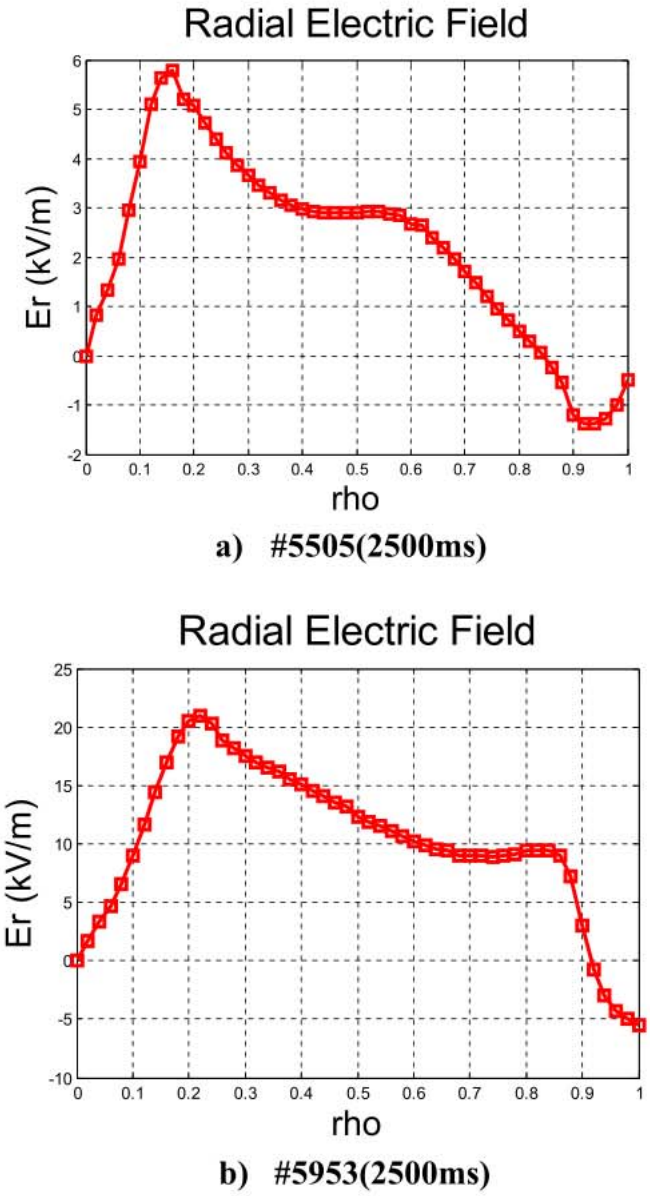

FIG. 6. Radial electric fields predicted by the extended rotation theory. (a) #5505 (2500 ms); (b) #5953 (2500 ms).

$$\bar{E}_r \quad V_{thj}\bar{B}_\theta\left[\hat{V}_{\theta j}\frac{\left\langle\frac{1}{1+\varepsilon\cos\xi}\right\rangle}{\left\langle\frac{1}{h_r}\right\rangle} \quad \hat{V}_{\phi j}\left(1+\frac{\partial R_0(r)}{\partial r}\right) \times \frac{\left\langle\frac{1}{(1+\varepsilon\cos\xi)}\frac{1}{h_r}\right\rangle}{\left\langle\frac{1}{h_r}\right\rangle} \quad \hat{P}'_j\right], \quad (21)$$

where $\hat{\bar{P}}_j' = \frac{\bar{P}_j'}{\bar{V}_{\theta j}} - \frac{1}{\bar{V}_{\theta j}} \frac{1}{n_j e_j \bar{B}_\theta} \frac{\partial \bar{P}_j}{\partial r}$. Converting Eq. (21) into the circular flux surface geometry, we get a more familiar (and more widely used) form for $\bar{E}_r$ calculation, Eq. (22), but still with the Shafranov shifts accounted for.

$$\bar{E}_r \quad \frac{1}{\bar{n}_j e_j} \frac{\partial \bar{P}_j}{\partial r} \quad \left[V_{\theta j} \bar{B}_\phi \quad V_{\phi j} \bar{B}_\theta \left(1 + \frac{\partial R_0(r)}{\partial r} \right) \right]. \qquad (22)$$

Thus, Eq. (21) coded in GTROTA[18] takes both the realistic Miller geometry[10] and Shafranov shift[9] effects into account.

VI. CONCLUSIONS

The extended neoclassical rotation theory[5 8] allows unprecedented neoclassical calculations of the poloidal asymmetries not only in density but also in velocity (both toroidal and poloidal) and electrostatic potential, thus neoclassically predicting both the inertial and gyroviscous transport contributions as functions of the asymmetries. Recently, neoclassical theories[24 26] were developed for the calculation of neoclassical toroidal viscosity (NTV) caused by the broken toroidal axisymmetry due to the perturbations in the toroidal magnetic field and were used to explain the velocity damping caused by the internal kink modes during ECH (Electron Cyclotron Heating) injections in the KSTAR.[27] In the KSTAR, a significant NTV damping comparable to the NBI torque is calculated[27] from the toroidal magnetic perturbations with its magnitude on the order of 10^{-3}. In comparison, the extended neoclassical rotation theory[7,8] takes the variations in the plasma parameters such as density, velocity, and electrostatic potential, along the poloidal direction into account and studies their neoclassical effects, which were translated into the neoclassical calculations of the Reynolds stress and gyroviscosity. Improved accuracy in the velocity predictions presented in this paper and Ref. 7 indicates the importance of these additional neoclassical momentum damping mechanisms in the accurate predictions of both the main ion and impurity transport in the modern tokamaks and the ITER (International Thermonuclear Experimental Reactor) as well. The magnitudes of the poloidal asymmetries calculated in this paper, summarized in Eq. (19), are much larger than the $O(10^{-3})$ non-axisymmetry in the toroidal magnetic field caused by the internal kink modes during the ECH injection.[27] Considering that V_θ is significantly smaller than V_ϕ, it is intuitively expected that the variations in poloidal direction must be much larger order of magnitude to introduce non-negligible damping effects, which is the case shown in this study.

The key factor that allows the extended theory[5 8] to neoclassically predict the asymmetries and the associated neoclassical transport comes from the unique characteristics of the S-S poloidal rotation model[12,13] applied in the development of the theory. GTROTA[18] with the recent upgrades has successfully analyzed two KSTAR H-mode discharges, which have limited velocity measurements compared to the DIII-D cases of Ref. 7, and predicted the important discharge parameters such as V_ϕ and V_θ profiles of both deuterium and carbon impurity with high accuracy, all the poloidal asymmetries in the S-S model,[12] and $\bar{E}_r$ as well. The predicted carbon toroidal velocities for the two KSTAR discharges agree very well with the measurements when the inertial and gyroviscous damping contributions are evaluated as functions of the asymmetries using the elongated flux surface geometry representation, which is the same finding as in Ref. 7. The predicted density asymmetries for the carbon impurity seem to correspond well with the experimental measurement reported[14,15] and are physically intuitive when considering the expected differences between the ohmic and the NBI-heated discharges, thus increasing the confidence in the predicted profiles of other asymmetries for the two KSTAR discharges investigated. With the asymmetries not only in density but also in velocity and electrostatic potential, we find that ν_{nj} is also a strong function of $V_{\phi j}^s$ but ν_{dj} is determined by a combination of the asymmetries and other plasma parameters. The extended rotation theory[7,8] is expected to be further extended in the near future to increase its accuracy in the plasma edge ($\rho > 0.9$) with a detailed atomic physics treatment and to investigate the mechanism of intrinsic rotations as well.

ACKNOWLEDGMENTS

The authors are grateful to the members of the KSTAR (Korea Superconducting Tokamak Advanced Research) team who made the measurements presented in this paper.

[1]P. A. Politzer, C. C. Petty, R. J. Jayakumar, T. C. Luce, M. R. Wade, J. C. DeBoo, J. R. Ferron, P. Gohil, C. T. Holcomb, A. W. Hyatt, J. Kinsey, R. J. L. Haye, M. A. Makowski, and T. W. Petrie, Nucl. Fusion **48**, 075001 (2008).
[2]R. J. Buttery, R. J. La Haye, P. Gohil, G. L. Jackson, H. Reimerdes, E. J. Strait, and the DIII-D team, Phys. Plasmas **15**, 056115 (2008).
[3]A. M. Garofalo, G. L. Jackson, R. J. L. Haye, M. Okabayashi, H. Reimerdes, E. J. Strait, J. R. Ferron, R. J. Groebner, Y. In, M. J. Lanctot, G. Matsunaga, G. A. Navratil, W. M. Solomon, H. Takahashi, M. Takechi, A. D. Turnbull, and the DIII-D team, Nucl. Fusion **47**, 1121 (2007).
[4]G. R. McKee, P. Gohil, D. J. Schlossberg, J. A. Boedo, K. H. Burrell, J. S. deGrassie, R. J. Groebner, R. A. Moyer, C. C. Petty, T. L. Rhodes, L. Schmitz, M. W. Shafer, W. M. Solomon, M. Umansky, G. Wang, A. E. White, and X. Xu, Nucl. Fusion **49**, 115016 (2009).
[5]W. M. Stacey, R. W. Johnson, and J. Mandrekas, Phys. Plasmas **13**, 062508 (2006).
[6]W. M. Stacey, *Fusion Plasma Physics*, 1st ed. (Wiley-VCH, John Wiley, Weinheim, Chichester, 2005), Chap. 10.
[7]C. Bae, W. M. Stacey, and W. M. Solomon, Nucl. Fusion **53**, 043011 (2013).
[8]W. M. Stacey, *Fusion Plasma Physics*, 2nd ed. (Wiley-VCH, John Wiley, Weinheim, Chichester, 2012), Chap. 10.
[9]L. L. Lao, S. P. Hirschman, and R. M. Wieland, Phys. Fluids **24**, 1431 (1981).
[10]R. L. Miller, M. S. Chu, J. M. Greene, Y. R. Lin-Liu, and R. E. Waltz, Phys. Plasmas **5**, 973 (1998).
[11]S. I. Braginskii, Rev. Plasma Phys. **1**, 205 (1965).
[12]W. M. Stacey, Phys. Plasmas **15**, 012501 (2008).
[13]W. M. Stacey, A. W. Bailey, D. J. Sigmar, and K. C. Shaing, Nucl. Fusion **25**, 463 (1985).
[14]M. L. Reinke, J. E. Rice, I. H. Hutchinson, M. Greenwald, N. T. Howard, J. W. Hughes, J. Irby, Y. Podpaly, J. L. Terry, and A. White, Nucl. Fusion **53**, 043006 (2013).
[15]K. D. Marr, B. Lipschultz, P. J. Catto, R. M. McDermott, M. L. Reinke, and A. N. Simakov, Plasma Phys. Controlled Fusion **52**, 055010 (2010).
[16]J. E. Rice, J. L. Terry, E. S. Marmar, and F. Bombarda, Nucl. Fusion **37**, 241 (1997).
[17]H. Chen, N. C. Hawkes, L. C. Ingesson, M. von Hellermann, K. D. Zastrow, M. G. Haines, M. Romanelli, and N. J. Peacock, Phys. Plasmas **7**, 4567 (2000).

[18]C. Bae, W. M. Stacey, and T. D. Morley, Comput. Phys. Commun. **184**, 2571–2587 (2013).
[19]M. Kwon, Y. K. Oh, H. L. Yang, H. K. Na, Y. S. Kim, J. G. Kwak, W. C. Kim, J. Y. Kim, J. W. Ahn, Y. S. Bae, S. H. Baek, J. G. Bak, E. N. Bang, C. S. Chang, D. H. Chang, I. Chavdarovski, Z. Y. Chen, K. W. Cho, M. H. Cho, W. Choe, J. H. Choi, Y. Chu, K. S. Chung, P. Diamond, H. J. Do, N. Eidietis, A. C. England, L. Grisham, T. S. Hahm, S. H. Hahn, W. S. Han, T. Hatae, D. Hillis, J. S. Hong, S. H. Hong, S. R. Hong, D. Humphrey, Y. S. Hwang, A. Hyatt, Y. K. In, G. L. Jackson, Y. B. Jang, Y. M. Jeon, J. I. Jeong, N. Y. Jeong, S. H. Jeong, H. G. Jhang, J. K. Jin, M. Joung, J. Ju, K. Kawahata, C. H. Kim, D. H. Kim, H.-S. Kim, H. S. Kim, H. K. Kim, H. T. Kim, J. H. Kim, J. C. Kim, J.-S. Kim, J.-S. Kim, K.-M. Kim, K. M. Kim, K. P. Kim, M. K. Kim, S. H. Kim, S. S. Kim, S. T. Kim, S. W. Kim, Y. J. Kim, Y. K. Kim, Y. O. Kim, W. H. Ko, Y. Kogi, J. D. Kong, S. Kubo, R. Kumazawa, S. W. Kwak, J. M. Kwon, O. J. Kwon, M. LeConte, D. G. Lee, D. K. Lee, D. R. Lee, D. S. Lee, H. J. Lee, J. H. Lee, K. D. Lee, K. S. Lee, S. G. Lee, S. H. Lee, S. I. Lee, S. M. Lee, T. G. Lee, W. C. Lee, W. L. Lee, J. Leur, D. S. Lim, J. Lohr, A. Mase, D. Mueller, K. M. Moon, T. Mutoh, Y. S. Na, Y. Nagayama, Y. U. Nam, W. Namkung, B. H. Oh, S. G. Oh, S. T. Oh, B. H. Park, D. S. Park, H. Park, H. T. Park, J. K. Park, J. S. Park, K. R. Park, M. K. Park, S. H. Park, S. I. Park, Y. M. Park, Y. S. Park, B. Patterson, S. Sabbagh, K. Saito, S. Sajjad, K. Sakamoto, D. C. Seo, S. H. Seo, J. C. Seol, Y. Shi, N. H. Song, H. J. Sun, L. Terzolo, M. Walker, S. J. Wang, K. Watanabe, A. S. Welander, H. J. Woo, I. S. Woo, M. Yagi, Y. Yaowei, Y. Yonekawa, K. I. Yoo, J. W. Yoo, G. S. Yoon, S. W. Yoon, and the KSTAR team, Nucl. Fusion **51**, 094006 (2011).
[20]W. M. Stacey and D. J. Sigmar, Phys. Fluids **28**, 2800 (1985).
[21]W. M. Stacey and C. Bae, Phys. Plasmas **16**, 082501 (2009).
[22]S. P. Hirshman and D. J. Sigmar, Nucl. Fusion **21**, 1079 (1981).
[23]W. A. Houlberg, K. C. Shaing, S. P. Hirshman, and M. C. Zarnstorff, Phys. Plasmas **4**, 3230 (1997).
[24]K. C. Shaing, M. S. Chu, C. T. Hsu, S. A. Sabbagh, J. C. Seol, and Y. Sun, Plasma Phys. Controlled Fusion **54**, 124033 (2012).
[25]J. K. Park, A. H. Boozer, and J. E. Menard, Phys. Rev. Lett. **102**, 065002 (2009).
[26]J. D. Callen, A. J. Cole, and C. C. Hegna, Nucl. Fusion **49**, 085021 (2009).
[27]J. Seol, S. G. Lee, B. H. Park, H. H. Lee, L. Terzolo, K. C. Shaing, K. I. You, G. S. Yun, C. C. Kim, K. D. Lee, W. H. Ko, J. G. Kwak, W. C. Kim, Y. K. Oh, J. Y. Kim, S. S. Kim, and K. Ida, Phys. Rev. Lett. **109**, 195003 (2012).